Journal of Magnetism and Magnetic Materials 579 (2023) 170880

Contents lists available at ScienceDirect

Journal of Magnetism and Magnetic Materials

journal homepage: www.elsevier.com/locate/jmmm

Research article

Magnon state transfer in chains with correlated disorder

M.S.S. Junior [a], W.V.P. de Lima [a,b], V.A. Teixeira [b], D.B. da Fonseca [b], F. Moraes [b], A.L.R. Barbosa [b], G.M.A. Almeida [a], F.A.B.F. de Moura [a,*]

[a] Instituto de Fisica, Universidade Federal de Alagoas, 57072-970, Maceio-AL, Brazil
[b] Departamento de Fisica, Universidade Federal Rural de Pernambuco, Recife-PE, 52171-900, Brazil

ARTICLE INFO

Keywords:
Magnon
Localization
Correlated disorder
Quantum information

ABSTRACT

We investigate a one-dimensional spin−1/2 quantum Heisenberg model with disordered exchange couplings and magnetic fields. The first features a correlated disorder obeying a power law spectrum of the form $S(k) \propto k^{-\beta}$. The magnetic fields are uniformly distributed random values. We numerically investigate the competition between disorder and correlation in a protocol involving the state transfer of a magnon state from one end of the chain to the other. The performance is measured via the transfer fidelity and end-to-end concurrence between spins. We address the conditions for a state transfer protocol to occur with good fidelities even in the presence of disorder.

1. Introduction

The dynamics of spin waves has attracted significant attention over the past decade due to their promising applications in information technology [1]. Spin waves are collective excitations of magnetic moments in magnetic materials. Besides giving birth to rich physics they offer an advantage over standard electronic transport in terms of energy dissipation [2]. Recent experimental works explore the use of magnons to control magnetic domain walls [3], form Bose–Einstein condensates [4], carry out efficient transport [5], and so forth [1].

Given their properties, spin waves also meet applications in quantum information processing [1,6]. Indeed, engineered spin chains have been a standard to the design of quantum-state transfer protocols [7]. Short- to moderate-distance transmission have been shown to be feasible in spin chains with static parameters that run on the natural time evolution of the system. As such, the topological profile of the system is crucial for delivering the desired output [8]. Long-range interacting spin chains have been investigated in [9,10]. In [10] the authors reduced it to an effective, ideal two-spin system which is scalable with the channel while keeping the interaction strength relatively high. Other configurations include staggered spin−1/2 chains [11,12] that display rich topological properties. Many-qubit quantum state transfer has also been explored [13].

There is a variety of configurations one can envisage to precise the speed, fidelity, and robustness of a qubit transfer [7,8,11,13–20]. One particular scheme relies on a minimum engineering of the channel by adjusting only the outer couplings [16,21]. Zwick et al. reported that the weak-coupling regime is quite robust against static disorder [19]. In Ref. [22], the authors showed that an inhomogeneous external field can extend the range of parameters that allows for high-fidelity state transfer in that class of spin chains.

Here we explore a 1D quantum Heisenberg spin−1/2 model featuring disordered exchange couplings and nonuniform magnetic fields. In particular, the spin–spin interaction assumes a correlated disorder distribution with power law spectrum $S(k) \propto k^{-\beta}$, with a tunable exponent β and k being the modulation wave vector. It was showed that correlated disorder can increase the quality of quantum state transfer protocols compared to the uncorrelated case [23]. We thus set out to investigate the interplay between disorder and correlations in a magnon transfer protocol. The magnetic field within the channel takes independent random values uniformly distributed in a given disorder width. At both ends of the chain, the magnetic fields are tunable parameters. These will be responsible for harnessing propagating magnon modes in the spectrum. The quantum state transfer works by preparing a magnon at one side of the chain, and letting it be reconstructed (as much as possible) at the other side via the Hamiltonian time evolution. The quality of the protocol can be measured by the transfer fidelity [7] and end-to-end concurrence [24]. Our results indicate that the presence of correlations in the disordered spin–spin coupling promotes good transfer fidelities under weak magnetic fields.

2. Model and formalism

Let us consider a quantum Heisenberg model with N spin−1/2 particles that reside on a linear chain under the effect of a nonuniform

* Corresponding author.
E-mail address: fidelis@fis.ufal.br (F.A.B.F. de Moura).

https://doi.org/10.1016/j.jmmm.2023.170880
Received 8 May 2023; Received in revised form 24 May 2023; Accepted 29 May 2023
Available online 1 June 2023

magnetic field $\vec{H}_n$. The Hamiltonian reads [25,26]

$$\mathcal{H} = -\sum_{n=1}^{N}\{J_n\vec{S}_n\cdot\vec{S}_{n+1} + \vec{H}_n\cdot\vec{S}_n\}, \tag{1}$$

where J_n are the exchange couplings connecting nearest-neighbor sites. The magnon transfer protocol occurs between the first and last sites of the chain ($n = 1$ and $n = N$) acting as sender and receiver, respectively. The exchange coupling between each of them and the channel (sites 2 through $N-1$) is set as $J_1 = J_{N-1} = j_0$. Now, the exchange couplings within the channel feature a kind of long-range correlated disorder [27]

$$J_n = \sum_{k=1}^{N/2} k^{-\beta/2}\cos\left(\frac{2\pi nk}{N} + \phi_k\right), \tag{2}$$

with ϕ_k being a random phase uniformly distributed in $[0, 2\pi]$. The series generated by the above formula is associated to the trace of a fractional Brownian motion with power spectrum $S(k) \propto k^{-\beta}$ [25,27].

The exponent β is a tunable parameter to control the degree of correlations. When $\beta = 0$, the couplings J_n are uncorrelated obeying a Gaussian distribution. For $\beta > 0$, long-range correlations set in and modifies the localization profile of the modes. Indeed, in an Anderson model featuring only diagonal disorder it has long been known that when $\beta > 2$, the series increments become persistent and it culminates in a localization–delocalization transition of single-particle eigenstates [27]. For the quantum Heisenberg model with disordered long-range correlated couplings, de Moura et al. [25] reported a mobility edge at the vicinity of $\beta = 1$ [28] separating extended and localized modes.

After generating the series according Eq. (2) we normalize the distribution and further $J_n \to [0.5\tanh(J_n) + J]$, where $J \equiv 1$ sets our energy scale. The nonuniform magnetic field within the channel are random numbers uniformly distributed with a disorder width h, that is $H_n \in [-h/2, h/2]$ for $n \neq 1, N$. Here we restrict our analysis to case of weak disorder $h < J$. The magnetic field acting on the outer spins is fixed to $H_1 = H_N = E_{SR}$.

Our computational basis is spanned by magnon states featuring a single reversed spin at a given location n, $|n\rangle = S_n^+|g\rangle$, where $|g\rangle$ denotes the ferromagnetic ground state. As such, an arbitrary superposition at time t reads $|\phi(t)\rangle = \sum_n f_n(t)|n\rangle$. The time-dependent Schrödinger equation is written as

$$(J_n + J_{n-1} + 2H_n)f_n - J_n f_{n+1} - J_{n-1}f_{n-1} = 2i\hbar\frac{df_n}{dt}. \tag{3}$$

Therefore, the time evolution of the state is given by ($\hbar = 1$) $|\phi(t)\rangle = e^{-i\mathcal{H}t}|\psi(0)\rangle$. All we need then is to perform a numerical diagonalization of the Hamiltonian to obtain all eigenvectors $|\psi_j\rangle = \sum_l c_l^j|l\rangle$ and eigenvalues E_j. Expanding the initial state in the eigenstate basis, $|\phi(0)\rangle = \sum_j A_j|\psi_j\rangle$, with $A_j = \sum_l f_l(0)c_l^j$, we get $f_n(t) = \sum_j A_j c_n^j e^{-iE_j t}$.

A single-qubit state can be encoded in the first site of the spin chain by preparing the input $|\phi(0)\rangle = c_0|g\rangle + c_1|1\rangle$. The actual state propagation takes place in the one-magnon subspace. Thus, a figure of merit of the protocol must include the transition amplitude to the other end of the chain $f_N(t)$. Indeed, if we average the output fidelity over all possible inputs $\{c_0, c_1\}$ (covering the whole Bloch sphere), we obtain a monotonic function of such a quantity amplitude, the so-called averaged fidelity

$$F(t) = \frac{1}{2} + \frac{|f_N(t)|}{3}\cos\xi + \frac{|f_N(t)|^2}{6}. \tag{4}$$

We set $\cos\xi = 1$ which is equivalent to a proper local rotation at the receiver's site. Such a fidelity ranges between 1/2 and 1.

The role of the tunable outer couplings j_0 is to induce an effective two-level dynamics between the outermost spins [16,21]. It happens when $j_0 \ll J$ and there is enough symmetry within the channel spectrum [8]. In other words, such a configuration can induce a pair of bilocalized eigenstates at both edges of the chain $|\psi^{\pm}\rangle \approx (|1\rangle \pm |N\rangle)/\sqrt{2}$. If this holds we expect pairwise entanglement to establish in between Rabi-like cycles. The concurrence [24] between the communicating parties in the single-excitation subspace reads

$$C(t) = 2|f_1(t)f_N(t)|, \tag{5}$$

which goes from 0 (no entanglement) to 1 (maximum entanglement).

In the absence of disorder, weak coupling models deliver quantum state transfer at time $\tau = j_0/\delta\lambda$, where $\delta\lambda$ is the gap between the bilocalized states [8,16,21]. This gap is typically small. A perturbative approach yields $\delta\lambda \propto j_0^2$ [21]. The proportionality constant here is a parameter that depends on the coupling profile of the channel [8]. For a uniform channel, it is simply $1/J$. The disordered spin chain addressed in this work features about the same order of magnitude. But the fluctuations in the spectrum induced by the disorder will affect the transfer time. Therefore, in our simulations we evaluate the maximum fidelity $F_{\max}$ and concurrence $C_{\max}$ in a wide time window up to $tJ = 10^6$ (we shall omit $J \equiv 1$ hereafter). This is more than compatible with the values of j_0 employed here. All those quantities are further averaged over many independent realizations of disorder.

3. Results

We emphasize that the quality of the quantum state transfer depends both on the strength of j_0 and the nature of eigenstates populating the channel spectrum. They are dramatically affected by the exponent β [27]. To address the matter let us analyze the eigenstates of the channel using the function $d(E_j) = N(|a_j| - |b_j|)$ which, for a given eigenvalue E_j, $|a_j|$ and $|b_j|$ represent the maximum and the minimum amplitudes, respectively. For extended states $|a_j| \approx |b_j|$ rendering $d(E_j)$ becomes smaller and roughly independent of N. For localized eigenstates, $d(E_j)$ increases with N. Therefore, using this topological measure we can detect extended modes throughout the spectrum.

By applying exact diagonalization to the disordered channel, we display the function $d = d(E)$ for $\beta = 0, 0.5, 1.5, 3$, and many system sizes in Fig. 1. For now we are taking $h = 0$, i.e., there is no external magnetic field. We can see that when $\beta > 1$ all curves for $E < 1$ collapse to a plateau. That is, the quantity does not depend on N, which is a clear signature of extended magnon modes. For $E > 1$, we observe that $d(E)$ increases with N. This behavior indicates the presence of localized modes. This sharp division is the result of strong long-range correlations that set in as soon as $\beta > 1$ [25,28]. If $\beta < 1$, the system only exhibit extended states in the vicinity of the uniform mode ($E = 0$). Next, we address how a quantum state transfer protocol can take place by harnessing propagating magnon modes.

We are now set to investigate the magnon transfer from one end of the chain to the other. First, it is important that we tune the local magnetic fields of sites 1 and N in resonance with a given energy of the channel spectrum that supports extended states. We choose $E_{SR} = 0.5$ in all simulations below.

In order to evaluate the input-averaged fidelity in Eq. (4), we set an initial state with $f_n(t = 0) = \delta_{n,1}$. Fig. 2 shows a histogram of the maximum fidelity $F_{\max}$ obtained in a time interval $t \in [0, 10^6]$ on a chain with $N = 60$ sites, with the weak coupling $j_0 = 0.01$ and null magnetic field $h = 0$. At this point we want to highlight the role of the long-range correlation alone. Many values of β is considered. When $\beta < 1$, the probability distribution is wide, with high-fidelity transfers being extremely rare. As discussed earlier, this is a consequence of the absence of magnon extended modes around $E = 0.5$. Even if the time evolution fails to deliver $|f_N| \approx 1$ in that case, we point out to the fact that the dynamics is still occurring almost exclusively in the subspace spanned by $|1\rangle$ and $|N\rangle$ [21,23]. Their effective local energies, however, is out of tune due to the spatial profile of localized states and the lack of particle–hole symmetry in the spectrum of the channel [8]. Even with the absence of the disordered magnetic field, the diagonal terms of the Hamiltonian [Eq. (1)] involves a sum of exchange couplings J_n and J_{n-1}, which are correlated random numbers. For $\beta > 1$ in Fig. 2, the performance improves dramatically and even more so when $\beta > 2$.

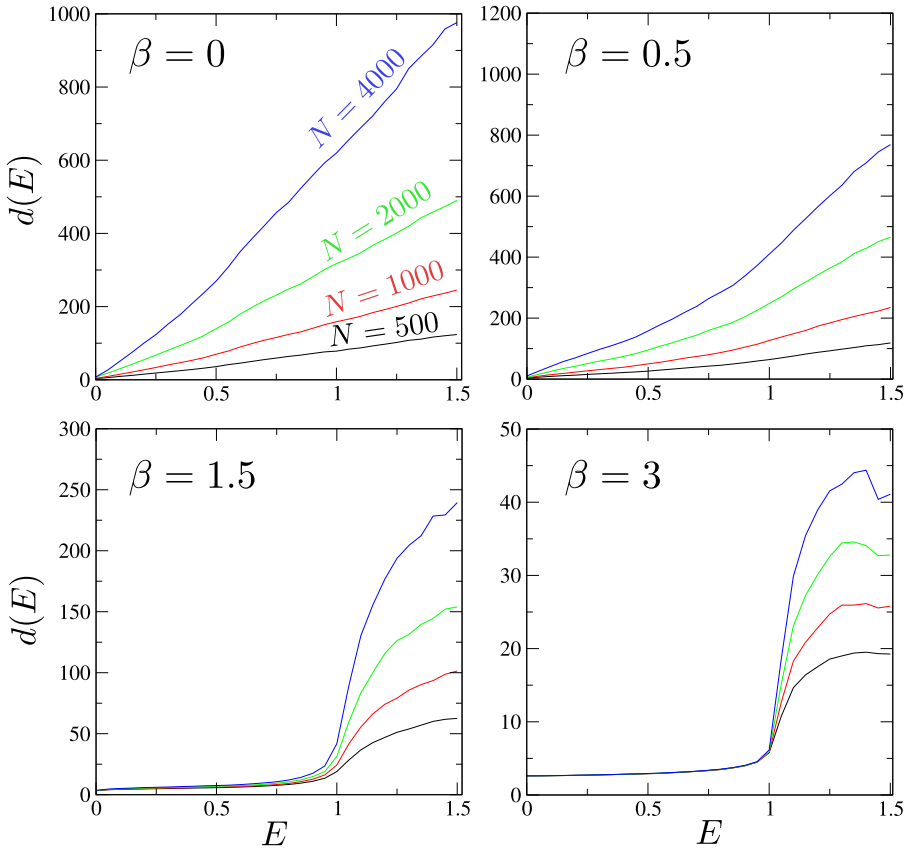

Fig. 1. Function $d(E)$ versus energy E in the absence of the magnetic field ($h = 0$). For a given eigenvalue this quantity reads $d(E_j) = N(|a_j| - |b_j|)$, with $|a_j|$ ($|b_j|$) being the largest (smallest) eigenfunction amplitude. Each panel depicts a different value of the correlation exponent β. Various system sizes are considered and each curve is averaged over 500 distinct disorder realizations.

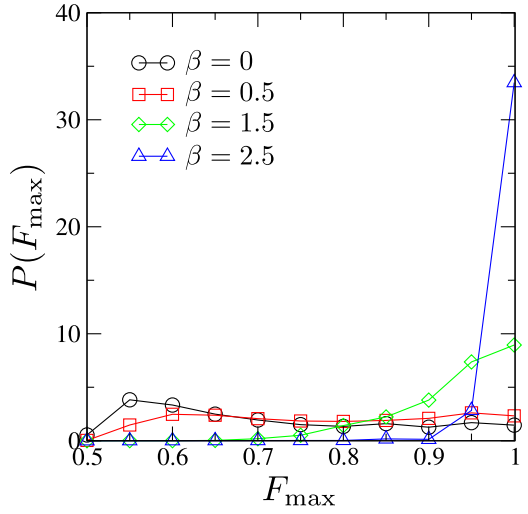

Fig. 2. Probability distribution of the maximum fidelity $P(F_{\max})$ versus $F_{\max}$. Calculations are done considering $N = 60$, $j_0 = 0.01$, $h = 0$, $E_{SR} = 0.5$ and many values of β. Data are obtained for 3000 independent disorder realizations.

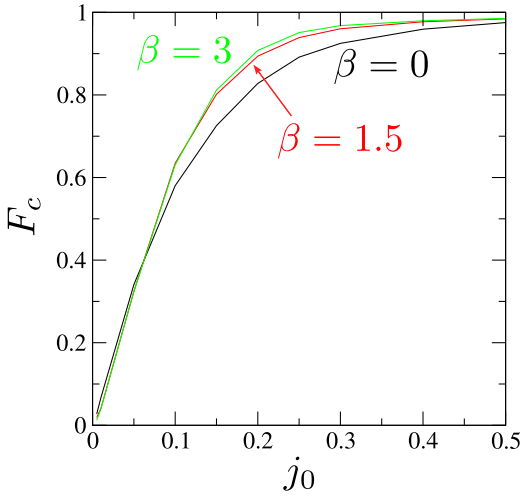

Fig. 3. Total occupation probability of the channel $F_c = \sum_{n=2}^{N-1} |f_n|^2$ versus j_0 for $N = 60$, $E_{SR} = 0.5$, $h = 0$, $\beta = 0, 1.5, 3$. Curves are averaged over 3000 independent disorder realizations.

Now, despite the presence of disorder, the vast majority of the samples (about 35% out of 3000 independent disorder realizations) provides fidelities above 0.95.

To see that the channel is barely populated during the realization of the protocol provided that $j_0 \ll 1$, regardless of the outcome fidelity, we evaluate $F_c = \sum_{n=2}^{N-1} |f_n|^2$. This accounts for total occupation probability within the channel. Results are shown in Fig. 3, where we plot F_c versus j_0 for distinct values of $\beta = 0, 1.5, 3$. We see that the formation of a two-level subspace is not affected by the correlation degree β. But as j_0 increases, the initial delta-located magnon will disperse into the channel. The two-level effective description no longer holds and the quantum state transfer becomes unfeasible. This is shown in Fig. 4 for the same parameters considered before, now including the disordered magnetic field with widths $h = 0.2$ and $h = 0.4$. The decaying trend looks similar in all cases albeit with different scaling

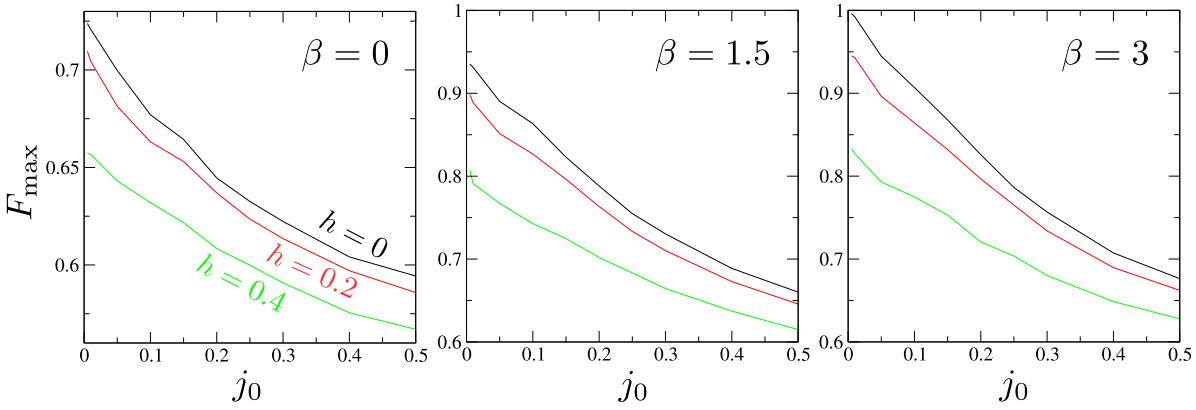

Fig. 4. $F_{\max}$ versus outer weak couplings j_0 for $N = 60$, $E_{SR} = 0.5$, $h = 0, 0.2, 0.4$, and $\beta = 0, 1.5, 3$. Curves are averaged over 3000 disorder realizations.

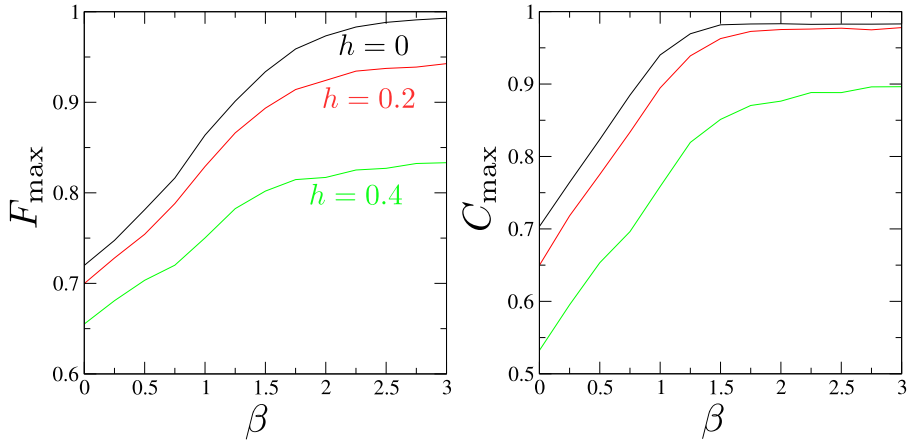

Fig. 5. Maximum fidelity $F_{\max}$ and maximum concurrence $C_{\max}$ versus β for $N = 60$, $E_{SR} = 0.5$, $j_0 = 0.01$, $h = 0, 0.2, 0.4$. Both quantities are averaged over 3000 independent disorder realizations.

parameters. We remark that the disordered magnetic field affects the transfer performance more severely, even when β is large.

Fig. 5 shows the dependence of $F_{\max}$ and $C_{\max}$ on β in more detail. It confirms that both quantities are correlated, meaning that bipartite entanglement between the first and last spins eventually builds up with the fidelity. Another interesting detail is that the performance gain induced by the long-range correlations reaches a limit for $\beta > 2$. Such a saturated level is set by the residual uncorrelated disorder due to the magnetic fields. That is, as long-range correlations work out to reduce the local variance [27] of the diagonal terms of the Hamiltonian [Eq. (1)], the uncorrelated series delivered by H_n eventually overcomes. Anderson localization then becomes relevant in the channel spectrum. Yet, it is possible to obtain fidelities higher than the bound corresponding to a classical transmission of a quantum state, $F = 2/3$, even for disorder widths as large as $h = 0.4$.

At last, we analyze how the performance scales with the size of the system N. Fig. 6 shows such a dependence for $N = 60$ up to 160, with fixed $E_{SR} = 0.5$, $j_0 = 0.01$, $h = 0.2$, and $\beta = 1.5, 3$. Both the fidelity and concurrence are damaged as N increases. This is due to the fact that j_0 is constant. The number of modes grows with N and so the density of states surrounding the energy level $E = 0.5$ to which sender and receiver spins are tuned. (This does not occur, for instance, in a family of chains that features a topological gap [11].) Still, once again the fidelities obtained for the system sizes considered in Fig. 6 under the influence of the two sources of disorder is higher than the classical threshold $F = 2/3$.

As N increases, if the same level of fidelity (or a greater one) is desired j_0 must be adjusted accordingly. A consequence of reducing j_0 is that the perturbative coupling between the outermost spins responds $\propto j_0^2$. It ultimately renders the transfer time to increase $\propto j_0^{-2}$. Hence, there is a physical constraint over the system size N. And it should be set in accordance with the desired speed/fidelity of the quantum state transfer protocol.

Quantum state transfer protocols can be seen as engineered quantum walks [29]. As such, the spin Hamiltonian employed here is realizable in devices that allow for a reasonable degree of tuning of the key parameters, namely couplings between adjacent sites and local frequencies. In this regard, photonic waveguide arrays are suitable platforms, with proof-of-principle realizations reported in [30,31] (see also Ref. [32] for a 2D simulations of a quantum walk). In [31] Chapman et al. implemented a perfect quantum state transfer protocol that demands a judicious tuning of all the couplings [15]. Note that the engineering requirements for the system presented here would much less demanding due to disorder, except for the parameters pertaining to the first and last sites. Another potential platform to host a variety of quantum communication protocols and also simulate spin systems is based on arrays of superconducting qubits, as shown recently in [33] for a programmable processor involving 62 qubits.

4. Conclusions

Some degree of disorder is inevitable in spin chains. Therefore, a proper design of solid-state devices to carry out quantum information protocols must take its various forms into account. Here, we have explored a one-dimensional Heisenberg spin−1/2 model as a quantum state transfer channel against the influence of disordered magnetic fields and exchange couplings. The latter features a long-range correlated disorder controlled by a parameter β. The magnetic fields are

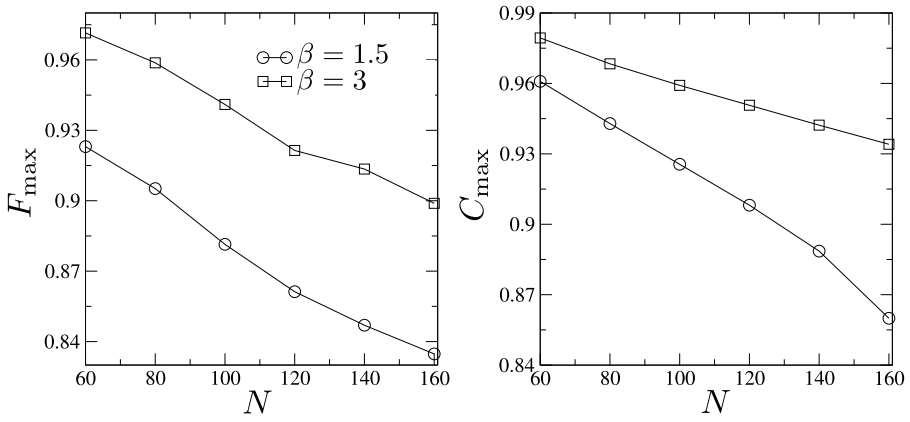

Fig. 6. Maximum fidelity $F_{\max}$ and maximum concurrence $C_{\max}$ versus system size N. System parameters are $E_{SR} = 0.5$, $j_0 = 0.01$, $h = 0.2$, $\beta = 1.5$ and 3. Curves are averaged over 3000 distinct disorder realizations.

random following a box-like distribution of width h. The competition between these two sources of disorder is crucial in defining the quality of the protocol. The qubit to be transmitted is encoded in a magnon state created on a ferromagnetic ground state. When $h = 0$ and $\beta > 2$, nearly perfect state transfer is achieved. This is possible due to the presence of extended states within the channel [23,27]. Anderson localization is induced upon setting $h \neq 0$, what deteriorates the overall quality of the transfer. However, better-than-classical transmission is still possible for moderate h.

CRediT authorship contribution statement

M.S.S. Junior: Conceptualization, Methodology, Software, Calculations. **W.V.P. de Lima:** Numerical calculations, Validation. **V.A. Teixeira:** Numerical calculations, Validation. **D.B. da Fonseca:** Numerical calculations, Validation. **F. Moraes:** Writing – review & editing. **A.L.R. Barbosa:** Writing – review & editing. **G.M.A. Almeida:** Writing – review & editing. **F.A.B.F. de Moura:** Conceptualization, Methodology, Numerical calculations, Writing – review & editing.

Declaration of competing interest

The authors declare the following financial interests/personal relationships which may be considered as potential competing interests: Francisco Anacleto Barros Fidelis de Moura reports financial support was provided by Federal University of Alagoas.

Data availability

Data will be made available on request.

Acknowledgments

This work was supported by CNPq, CNPq-Rede Nanobioestruturas, CAPES, FINEP (Federal Brazilian Agencies), FAPEAL (Alagoas State Agency), and FACEPE (Pernambuco State Agency).

References

[1] H.Y. Yuan, Y. Cao, A. Kamra, R.A. Duine, P. Yan, Phys. Rep. 965 (2022) 1.
[2] M. Amundsen, I.V. Bobkova, A. Kamra, Phys. Rev. B 106 (2022) 144411.
[3] J. Han, et al., Science 366 (2019) 1121.
[4] B. Divinskiy, et al., Nat. Commun. 12 (2021) 6541.
[5] T. Wimmer, et al., Phys. Rev. Lett. 123 (2019) 257201.
[6] O. Marchukov, et al., Nat. Commun. 7 (2016) 13070.
[7] S. Bose, Phys. Rev. Lett. 91 (2003) 207901.
[8] G.M.A. Almeida, Phys. Rev. A 98 (2018) 012334.
[9] M. Avellino, A.J. Fisher, S. Bose, Phys. Rev. A 74 (2006) 012321.
[10] G. Gualdi, V. Kostak, I. Marzoli, P. Tombesi, Phys. Rev. A 78 (2008) 022325.
[11] G.M.A. Almeida, F. Ciccarello, T.J.G. Apollaro, A.M.C. Souza, Phys. Rev. A 93 (2016) 032310.
[12] P. Serra, A. Ferrón, O. Osenda, J. Phys. A 55 (2022) 405302.
[13] T.J.G. Apollaro, et al., Phys. Scr. 2015 (2015) 014036.
[14] M.B. Plenio, J. Hartley, J. Eisert, New J. Phys. 6 (2004) 36.
[15] M. Christandl, N. Datta, A. Ekert, A.J. Landahl, Phys. Rev. Lett. 92 (2004) 187902.
[16] A. Wojcik, T. Luczak, P. Kurzynski, A. Grudka, T. Gdala, M. Bednarska, Phys. Rev. A 72 (2005) 034303.
[17] L. Banchi, T.J.G. Apollaro, A. Cuccoli, R. Vaia, P. Verrucchi, New J. Phys. 13 (2011) 123006.
[18] G. Gualdi, I. Marzoli, P. Tombesi, New J. Phys. 11 (2009) 063038.
[19] A. Zwick, G.A. Álvarez, J. Stolze, O. Osenda, Quantum Inf. Comput. 15 (2015) 582.
[20] D. Messias, C.V.C. Mendes, G.M.A. Almeida, M.L. Lyra, F.A.B.F. de Moura, J. Magn. Magn. Mater. 505 (2020) 166730.
[21] A. Wojcik, T. Luczak, P. Kurzynski, A. Grudka, T. Gdala, M. Bednarska, Phys. Rev. A 75 (2007) 022330.
[22] G.L. Giorgi, T. Busch, Phys. Rev. A 88 (2013) 062309.
[23] G.M.A. Almeida, F.A.B.F. de Moura, M.L. Lyra, Phys. Lett. A 382 (2018) 1335.
[24] W.K. Wootters, Phys. Rev. Lett. 80 (1998) 2245.
[25] F.A.B.F. de Moura, M.D. Coutinho-Filho, E.P. Raposo, M.L. Lyra, Phys. Rev. B 66 (2002) 014418.
[26] Y.A. Kosevich, V.V. Gann, J. Phys.: Condens. Matter 25 (2013) 246002.
[27] F.A.B.F. de Moura, M.L. Lyra, Phys. Rev. Lett. 81 (1998) 3735.
[28] J.P. Santos Pires, N.A. Khan, J.M. Viana Parente Lopes, J.M.B. Lopes dos Santos, Phys. Rev. B 99 (2019) 205148.
[29] R. Herrman, T.S. Humble, Phys. Rev. A 100 (2019) 012306.
[30] M. Bellec, G.M. Nikolopoulos, S. Tzortzakis, Opt. Lett. 37 (2012) 4504.
[31] R. Chapman, et al., Nature Commun. 7 (2016) 11339.
[32] H. Tang, et al., Sci. Adv. 4 (2018) eaat3174.
[33] M. Gong, et al., Science 372 (2021) 948.